

A Source–Receptor Perspective on the Polar Hydrologic Cycle: Sources, Seasonality, and Arctic–Antarctic Parity in the Hydrologic Cycle Response to CO₂ Doubling

HANSI K. A. SINGH

Atmospheric Sciences and Global Change Division, Pacific Northwest National Laboratory, Richland, Washington

CECILIA M. BITZ

Department of Atmospheric Sciences, University of Washington, Seattle, Washington

AARON DONOHOE

Applied Physics Laboratory, University of Washington, Seattle, Washington

PHILIP J. RASCH

Atmospheric Sciences and Global Change Division, Pacific Northwest National Laboratory, Richland, Washington

(Manuscript received 28 December 2016, in final form 31 August 2017)

ABSTRACT

Numerical water tracers implemented in a global climate model are used to study how polar hydroclimate responds to CO₂-induced warming from a source–receptor perspective. Although remote moisture sources contribute substantially more to polar precipitation year-round in the mean state, an increase in locally sourced moisture is crucial to the winter season polar precipitation response to greenhouse gas forcing. In general, the polar hydroclimate response to CO₂-induced warming is strongly seasonal: over both the Arctic and Antarctic, locally sourced moisture constitutes a larger fraction of the precipitation in winter, while remote sources become even more dominant in summer. Increased local evaporation in fall and winter is coincident with sea ice retreat, which greatly augments local moisture sources in these seasons. In summer, however, larger contributions from more remote moisture source regions are consistent with an increase in moisture residence times and a longer moisture transport length scale, which produces a robust hydrologic cycle response to CO₂-induced warming globally. The critical role of locally sourced moisture in the hydrologic cycle response of both the Arctic and Antarctic is distinct from controlling factors elsewhere on the globe; for this reason, great care should be taken in interpreting polar isotopic proxy records from climate states unlike the present.

1. Introduction

A thorough understanding of the polar hydrologic cycle response to CO₂-induced warming is essential for advancing study of both the global hydrologic cycle and the climate of the polar regions. The polar regions are tightly coupled to the extrapolar regions through the meridional transfer of heat, moisture, and momentum. As a result, it is not surprising that the polar climate response to greenhouse gas forcing is, at least in part, dependent on changes in meridional transport. At the

same time, changes in polar sea ice cover portend changes in local moisture availability through evaporation. In this study, we use source–receptor methods to explore how changes in both the meridional transport of moisture and local evaporation contribute to the polar hydrologic cycle response to CO₂ doubling.

Moisture transport is a crucial component of meridional moist static energy (MSE) transport. Transport of MSE moderates the pole-to-equator temperature gradient, determines the amount of moisture available at the surface (precipitation minus evaporation), and affects atmospheric dynamics at the largest spatial scales. Observational studies of polar hydroclimate

Corresponding author: Hansi K. A. Singh, hansi.singh@pnnl.gov

have generally focused on moisture transport from the extrapolar regions, since the majority of polar precipitable water originates remotely (Peixoto and Oort 1992; Overland and Turet 1994). In both the Arctic and Antarctic, variations in moisture transport are evident (Slonaker and Woert 1999; Groves and Francis 2002; Jakobson and Vihma 2010), with particular transport pathways linked to regional cyclone activity in the Arctic (Sorteberg and Walsh 2008). Variability of polar moisture transport with the annular mode has also been noted in both hemispheres (Noone and Simmonds 2002; Groves and Francis 2002; Oshima and Yamazaki 2004).

Today, the polar regions are changing rapidly in response to anthropogenic forcings. Observational studies of increased river discharge into the Arctic (Peterson et al. 2002; Zhang et al. 2013) and decreased high-latitude ocean salinity (Boyer et al. 2005; Helm et al. 2010; Durack and Wijffels 2010; Durack et al. 2012; Levitus et al. 2013) imply that moisture convergence into the high latitudes is increasing (though ice cap melt also plays a role; see, e.g., Shepherd et al. 2004; Peterson et al. 2006). Projections of hydrologic cycle intensification with CO₂-induced warming suggest that moisture transport into the polar regions should intensify as the planet warms (Held and Soden 2006) and that this intensification is primarily due to the thermodynamic increase in atmospheric moisture (Held and Soden 2006; Skific et al. 2009). Multimodel comparison studies also agree that moisture transport into the polar regions will increase as the planet warms (Hwang and Frierson 2010; Bengtsson et al. 2011).

Though changes in high-latitude moisture transport have been the primary focus of most studies on the polar hydroclimate response to CO₂-induced warming, the role of sea ice retreat in amplifying the hydrologic cycle remains an important, though less understood, factor. Sea ice retreat is a central player in how polar climates respond to anthropogenic forcings and is linked to a variety of positive feedbacks that tend to amplify polar warming (Holland and Bitz 2003; Screen and Simmonds 2010; Serreze and Barry 2011). Bintanja and Selten (2014) were the first to identify the role of sea ice loss and increased local evaporation as a major part of the Arctic hydroclimate response to CO₂-induced warming. While their study emphasized the role of increased locally sourced evaporation to the polar hydrologic cycle response to CO₂-induced warming [representative concentration pathway 8.5 and 4.5 (RCP8.5 and RCP4.5) scenarios from 37 participating models in the IPCC Fifth Assessment Report (AR5); see IPCC 2013], there was a key factor that made their conclusions equivocal. Because Bintanja and Selten (2014) utilized

budget methods, not source–receptor methods, they were unable to decompose the net moisture transport into the polar cap into local moisture exported from the Arctic (i.e., moisture evaporated from the Arctic that precipitates outside the Arctic) and remote moisture imported into the Arctic (i.e., moisture evaporated from outside the Arctic that precipitates within the Arctic). Since some nonzero fraction of moisture evaporated from the polar regions is exported from the polar regions and precipitates elsewhere, estimates of locally and remotely sourced moisture in Bintanja and Selten (2014) were unavoidably biased toward local sources and against remote ones.

Here, we use a single GCM equipped with numerical water tracers to show that the (climatological) local versus remote contribution to Arctic precipitation may be biased to first order using budget methods, such as used in Bintanja and Selten (2014), Zhang et al. (2013), and Bengtsson et al. (2011). Nevertheless, source–receptor methods are not a panacea. While source–receptor methods permit the local and remote contributions to the polar precipitation to be diagnosed with greater accuracy than budget methods, they must be carefully implemented using Eulerian or Lagrangian formulations in a single climate model; since individual models may have large hydrologic cycle biases, results from source–receptor studies, like this one, may also have large biases due to uncertainties in the hydrologic cycle of the single model used.

Because of the ease and the potential for multimodel comparisons, most previous studies have relied on Eulerian budget methods to estimate the relative role of local (i.e., evaporated within the polar cap) and remote (i.e., evaporated outside the polar cap) moisture sources to polar precipitation. Most studies using source–receptor methods to ascertain polar moisture source provenance have done so for isotope calibration purposes to aid in the interpretation of paleo-proxy records (see, e.g., Johnsen and White 1989; Koster et al. 1992; Ciais et al. 1995; Werner et al. 2001). More recently, Vázquez et al. (2016) used Lagrangian back-trajectory methods to quantify sources of Arctic precipitation; Sodemann and Stohl (2009) performed a similar Lagrangian back-trajectory analysis of Antarctic precipitation sources. As far as we know, no moisture transport studies have yet considered how polar precipitation-source provenance evolves as the planet warms.

In this study, we consider how the polar hydrologic cycle responds to CO₂-induced warming from a source–receptor perspective. Numerical water tracers (WTs) are implemented in a global climate model (GCM) that permits aerial moisture to be traced from its point of evaporation (its source region) to precipitation (its sink region, i.e., receptor). In brief, WTs allow aerial moisture to be labeled with its (tagged) region of origin; this

tag is maintained through the course of this water molecule's journey through the model atmosphere, including advection and phase changes, and is removed (i.e., "renewed") upon precipitation onto a land or ocean surface. As a result, precipitation at each model grid point can be separated into contributions from each tagged source region (i.e., the different WTs).

Here, we use WTs implemented in a state-of-the-art GCM to disentangle seasonal changes in local and remote moisture source provenance for polar precipitation in a warmer world. We also attribute these changes in local and remote moisture source provenance by undertaking a perturbation analysis similar to that performed in Singh et al. (2016a), where the matrix operator framework for assessing the aerial moisture source–receptor relationship developed in Singh et al. (2016b) is used to assess the relative roles of changes in evaporation and changes in transport in hydrologic cycle changes due to CO₂ doubling. We contrast mechanisms underlying changes in polar hydroclimate with those underlying robust changes in the hydrologic cycle globally [as assessed in Singh et al. (2016a)]. Through our analysis, we tackle several open questions regarding how polar hydroclimate responds to CO₂-induced warming seasonally and the role of sea ice retreat in the hydroclimate response.

This study is organized as follows. We describe our methods and experimental setup in section 2. We begin our analysis of polar moisture source provenance by considering the mean state in section 3a and proceed to the hydrologic cycle response to CO₂ doubling in section 3b. In section 3c, we consider the mechanisms driving changes in the polar water cycle and focus on changes in locally sourced evaporation coincident with sea ice retreat in section 3c. We discuss our results and offer some concluding remarks in section 4.

2. Methods

The control and CO₂-doubling WT experiments are as described previously in Singh et al. (2016a,b), with the following three paragraphs closely following text from the original sources.

We use the fully coupled Community Earth System Model, version 1.0 (CESM1; Hurrell et al. 2013) with all model components at 1° spatial resolution. The atmosphere component, the Community Atmosphere Model, version 5.0 (CAM5.0; Neale et al. 2012), has been refined to include water tracing capability. WT implementation is similar to that described in Koster et al. (1986), Joussaume et al. (1986), and Bosilovich and Schubert (2002). Water evaporated (or sublimated) over each tagged region is tracked in all aspects of the model's hydrologic cycle, including surface fluxes, condensation processes, and

atmospheric transport. Evaporation and sublimation are assumed to be across the gradient of individual tagged water types at the surface and the lowest model level (see, e.g., Winschall et al. 2014). The advected tracer quantity used for each tagged water type at each grid point and atmospheric level is the ratio of the mass of the total tagged water type to the mass of the air. For water vapor only, this is equivalent to the specific humidity of the tagged water type, although cloud liquid and cloud ice are advected as well. Transport by boundary layer turbulence and large-scale advection occurs without loss, and thus the tagged water types are treated as conservative tracers. Being passive tracers, the WTs do not affect the mean state climate or any of the variables therein, and are evolved by the modeled atmospheric dynamics and physics.

An equilibrium preindustrial experiment is performed with this tagged version of CESM1(CAM5). Model biases in the CESM1(CAM5) preindustrial hydrologic cycle have been assessed (see, e.g., Yang et al. 2013; Wehner et al. 2014; Qian et al. 2015) and are most prominent in the tropics. To assess moisture sources and seasonality in the CESM, aerial water is tagged with its region of origin in 10° latitude bands over each ocean basin. Each continent is tagged separately, with Eurasia and North America subdivided into two parts each. There are 49 distinct tagged regions in total, encompassing the entire globe. To assess the hydrologic cycle response to quasi-equilibrium CO₂ doubling, a second experiment is branched from the pre-industrial control simulation in which atmospheric CO₂ is doubled from its preindustrial concentration of approximately 290–580 ppm. The simulation is run without WTs for 270 yr to approach a quasi-equilibrium state. For a final 30 yr, WTs with the same spatial configuration as for the control experiment are introduced. The net top-of-atmosphere energetic imbalance over this final 30-yr period is approximately 0.1 W m⁻².

December–February (DJF), March–May (MAM), June–August (JJA), and September–November (SON) seasonal climatologies from the control and CO₂-doubling experiment are created from 30 yr of model output with WTs. All differences are given as that between the CO₂-doubling experiment and the control. In all analyses, the Arctic is defined as all ocean north of 60°N and Greenland, and does not include any segments of North America or Eurasia; the Antarctic is defined as all land and ocean south of 60°S.

3. Results

a. The mean state polar moisture provenance

Many previous studies on polar hydroclimate have relied on budget methods for estimating local and

TABLE 1. Seasonal characteristics of the preindustrial Arctic hydrologic cycle (Sv), in terms of P (row 1), E (row 2), and moisture transport. Using numerical WTs, the net moisture transport (row 3) can be decomposed into the Arctic-sourced moisture that is exported from the Arctic (row 4) and the moisture from the rest of the globe that is imported into the Arctic (row 5), giving an estimate of the contribution of locally sourced moisture to Arctic P (row 6).

	DJF	MAM	JJA	SON
Total Arctic P	0.45	0.39	0.52	0.58
Total Arctic E	0.17	0.11	0.07	0.17
Net moisture transport into Arctic	0.28	0.28	0.45	0.41
Arctic-sourced E to rest of globe (moisture exported from Arctic)	0.05	0.04	0.03	0.06
Rest of globe-sourced E to Arctic (remote contribution to Arctic P)	0.33	0.32	0.48	0.47
Arctic-sourced E to Arctic (local contribution to Arctic P)	0.12	0.07	0.04	0.11

remote moisture sources (see, e.g., [Bintanja and Selten 2014](#); [Bengtsson et al. 2011](#); [Zhang et al. 2013](#)). In [Table 1](#), we show the advantage of employing a source–receptor framework for understanding changes in polar moisture source provenance. The total Arctic precipitation ([Table 1](#), row 1) is equal to the sum of the local evaporative flux ([Table 1](#), row 2) and the net moisture flux across some boundary latitude ([Table 1](#), row 3). Without the benefit of WTs, the local evaporative flux ([Table 1](#), row 2) is reckoned to be equal to the local contribution to the polar precipitation (i.e., the portion of the polar precipitation arising from moisture evaporated within the polar cap), while the net moisture flux across the boundary latitude ([Table 1](#), row 3) is reckoned to be equal to the remote contribution to the polar precipitation (i.e., the portion of the polar precipitation arising from moisture evaporated outside the polar cap). This approach assumes that all moisture evaporated from the polar regions also precipitates within the polar regions; in other words, moisture export from the polar regions is assumed to be negligibly small.

Source–receptor methods, on the other hand, do not make any prior assumptions regarding moisture export from the polar regions. The use of WTs allows the net moisture flux across the polar boundary to be subdivided into the locally evaporated moisture that is exported ([Table 1](#), row 4) and the remotely evaporated moisture that is imported ([Table 1](#), row 5). As a result, the local and remote contributions calculated using source–receptor methods are substantially different from those computed from conventional estimates (cf. [Table 1](#), rows 2, 3, with [Table 1](#), rows 6, 5). Indeed, our results show that the fraction of the locally evaporated moisture exported from the polar regions varies seasonally from nearly 30% in DJF to over 40% in JJA (though it is likely that the bounding latitude for the polar regions affects the magnitude of this export; more poleward latitudinal boundaries, for example, might be expected to have lower polar export fractions because of less transport by baroclinic eddies). Therefore, estimates that do not use source–receptor methods bias the local

contribution between 40% and 75% too high (in DJF and JJA) and bias the remote contribution between 5% and 15% too low (in JJA and DJF). In a future study, we will consider how modifying assumptions about moisture export from the polar regions affects observational estimates of polar moisture source provenance.

[Figure 1](#) shows the contribution of locally sourced moisture and remotely sourced moisture to Arctic ([Figs. 1a,c](#)) and Antarctic ([Figs. 1b,d](#)) precipitation [in Sv (1 Sv = 106 m³ s⁻¹) and in fraction of the total]. In both regions, remote moisture source regions provide most of the polar precipitation throughout the year. Over the Arctic, the fraction of the precipitation as a result of remote moisture sources ranges from a maximum of 90% in July to a minimum of 70% in January ([Fig. 1c](#)); for the Antarctic, this seasonal range of remotely sourced precipitation is smaller, from 85% in January to 80% in June and July ([Fig. 1d](#)). For the Arctic, local sources constitute the greatest fraction of the precipitation in winter (DJF), while for the Antarctic, this modest increase in locally sourced moisture in winter (JJA) is not evident. At most, local sources constitute 30% of the total monthly precipitation over the Arctic and 20% over the Antarctic.

Closer inspection of Arctic and Antarctic precipitation moisture source regions shows substantial differences in the seasonal cycle of moisture sources. The North Atlantic (between 50° and 70°N) is the largest moisture source region for the Arctic in winter, spring, and fall (DJF, MAM, and SON, respectively; [Figs. 2a,b,d](#)); in contrast, the North Pacific provides very little moisture to the Arctic over any season [consistent with the findings from [Vázquez et al. \(2016\)](#)]. This difference between the subpolar Atlantic and Pacific is likely driven by the greater temperature of the former, which enhances surface turbulent latent heat fluxes ([Hartmann 1994](#); [Yu and Weller 2007](#)); the northeast tilt of the jet and storm track over the Atlantic may also enhance moisture transport from the North Atlantic to the Arctic ([Woods et al. 2013](#)). The continents, particularly northern Eurasia and northern North America, are the

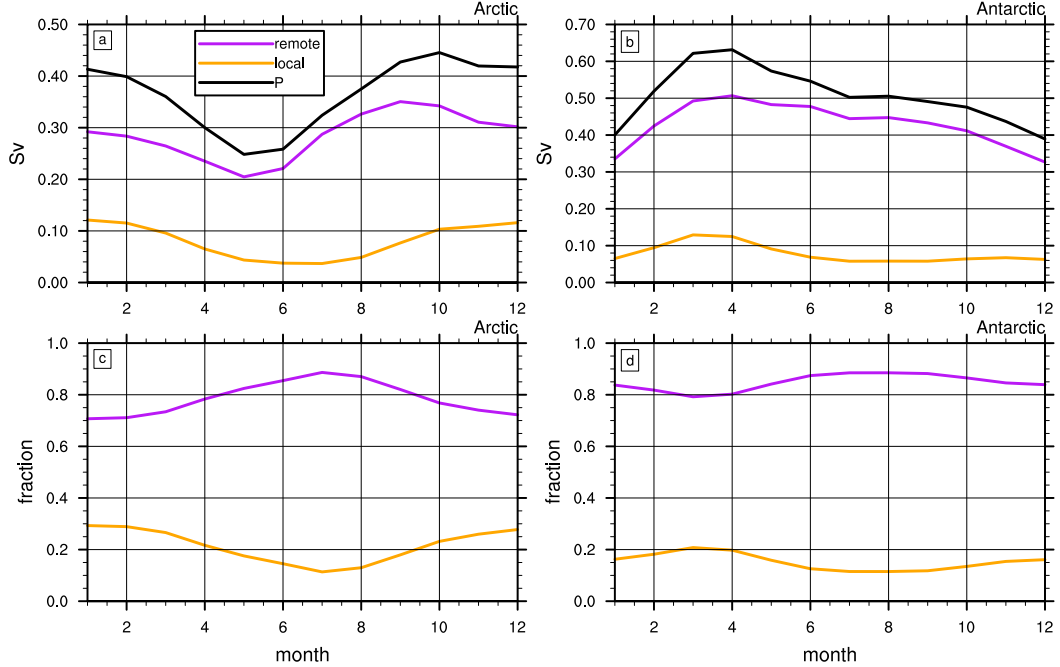


FIG. 1. Monthly contribution of local (orange) and remote (purple) moisture sources to the polar precipitation (black) in the preindustrial control run: contribution (Sv) to the (a) Arctic and (b) Antarctic precipitation, and fractional contribution to the (c) Arctic and (d) Antarctic precipitation.

largest sources of Arctic moisture in summer (JJA; Fig. 2c), when the contribution from the North Atlantic is much smaller than during the remainder of the year [similar to findings from Vázquez et al. (2016)]. The subtropical and midlatitude Atlantic and Pacific remain

significant Arctic moisture sources year-round (Fig. 2; also see Vázquez et al. 2016).

In comparison to the Arctic, the seasonal cycle of Antarctic precipitation source regions is muted, and these sources are relatively invariant year-round. Over

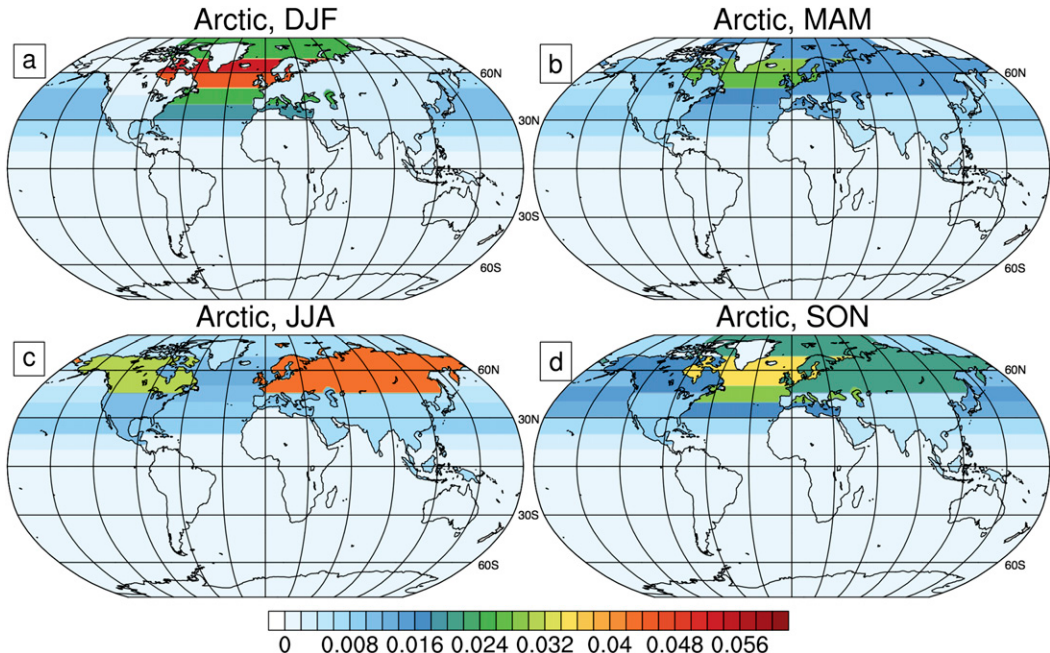


FIG. 2. Sources of Arctic precipitation (Sv) per tagged region, in (a) DJF, (b) MAM, (c) JJA, and (d) SON.

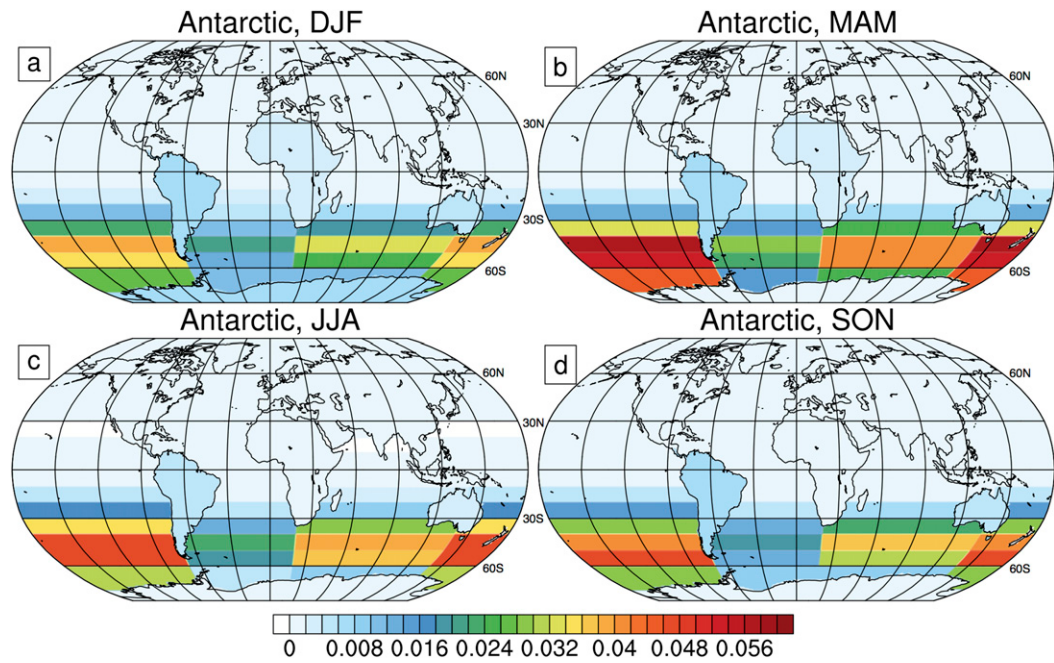


FIG. 3. As in Fig. 2, but for the Antarctic.

all seasons, the midlatitude Pacific is the largest contributor to polar precipitation, followed by the midlatitude Indian Ocean and midlatitude Atlantic. The greater size of the Pacific source is likely due to the greater zonal width of the Pacific tagged source region compared to the other basins. Seasonally, there is a modest equatorward shift in the mean source region between Antarctic winter (JJA; Fig. 3c) and summer (DJF; Fig. 3a), indicating that the moisture is transported further meridionally in summer than in winter [consistent with the results from Sodemann and Stohl (2009)].

b. Effect of CO_2 doubling on polar moisture source provenance

From a source–receptor perspective, the mean state hydrologic cycles in the Arctic and Antarctic differ substantively. In the Arctic, moisture source regions vary strongly between seasons (Fig. 2); the local contribution to Arctic precipitation is substantially smaller than the remote contribution during all seasons and peaks in winter (DJF; Figs. 1a,c). In the Antarctic, on the other hand, there is little seasonal variation in moisture source regions (Fig. 3), and there is no particular season in which local moisture sources dominate (Figs. 1b,d).

Though the mean state seasonal Arctic and Antarctic hydrologic cycles differ, we find that the seasonal response to CO_2 doubling is quite similar over both regions (Fig. 4). Over all seasons, polar precipitation increases in both hemispheres, consistent with increased

high-latitude moistening on a warmer planet (Manabe and Stouffer 1994; Held and Soden 2006). In summer (JJA for the Arctic and DJF for the Antarctic), the remote contribution to the precipitation increases most, while changes in the local contribution to the precipitation are minimal, constituting less than 10% of the total precipitation change; in winter (DJF for the Arctic; JJA for the Antarctic), on the other hand, the local contribution to the precipitation increases substantially, constituting 60% of the total change in precipitation in the Arctic and 35% in the Antarctic (Figs. 4c,d, respectively).

In Table 2 we contrast our estimate of changes in local and remote moisture source contributions to the Arctic precipitation using WTs with estimates that utilize budget methods, such as Bintanja and Selten (2014). With budget methods, the local contribution to the Arctic precipitation change is reckoned to be the change in the polar evaporation (Table 2, row 2), while the remote contribution is the change in the net moisture flux into the polar cap (Table 2, row 3). In this assessment, the local contribution is reckoned to be much greater than the remote contribution in winter (DJF) and of similar magnitude to the remote contribution in the shoulder seasons (MAM and SON); the remote contribution is found to exceed the local contribution only in summer (JJA). Annually, the local contribution to the precipitation change is found to be of similar magnitude to the remote contribution to the precipitation change.

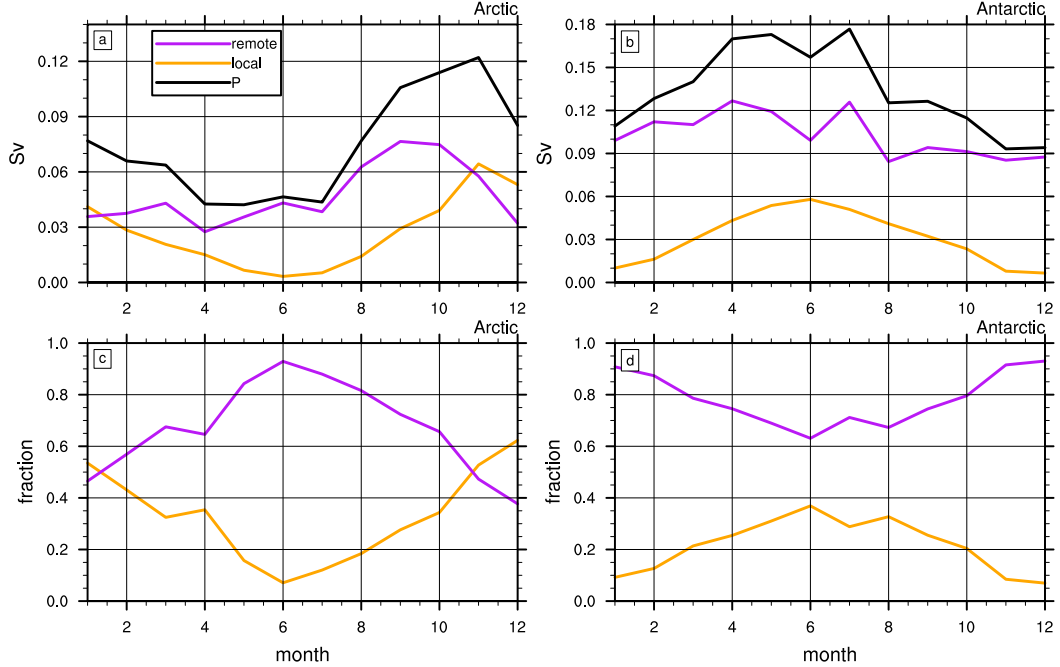


FIG. 4. As in Fig. 1, but for the change in the monthly contribution between the CO₂-doubling and preindustrial control runs.

Using WTs, on the other hand, we find that a substantial fraction of the increased local evaporation is exported from the Arctic (Table 2, row 4). With this information, the remote contribution to the Arctic precipitation change (Table 2, row 5) is greater than the local contribution to the Arctic precipitation change (Table 2, row 6) over summer (JJA) and the shoulder seasons (MAM and SON); the local and remote contributions are of similar magnitude only in winter (DJF). Using WTs we find that the remote contribution to the Arctic precipitation change with CO₂ doubling greatly exceeds the local contribution in the annual mean.

We now consider spatial patterns of changes in moisture source provenance in response to CO₂ doubling. Figures 5 and 6 show how the fraction of the total polar precipitation contributed by region *j* differs

between the CO₂-doubling and preindustrial control experiments:

Fractional change in *P* sourced from region *j*

$$= \frac{E_{j \rightarrow \text{polar}}^{2\text{XCO}_2}}{P_{2\text{XCO}_2, \text{polar}}} - \frac{E_{j \rightarrow \text{polar}}^{\text{Control}}}{P_{\text{Control}, \text{polar}}}, \quad (1)$$

where $E_{j \rightarrow \text{polar}}^X$ is the moisture contribution from region *j* that precipitates over the polar cap in experiment *X* (either the preindustrial control or the CO₂-doubling experiments) and $P_{X, \text{polar}}$ is the total precipitation over the polar cap in experiment *X*. Tables 3 and 4 show evaporative contributions and percentage of the total precipitation from key source regions for the Arctic and Antarctic, respectively.

TABLE 2. Arctic hydrologic cycle response (Sv) to CO₂ doubling, in terms of the change in precipitation ΔP (row 1), ΔE (row 2), and change in moisture transport. Using numerical WTs, the change in the net moisture transport (row 3) can be decomposed into the change in the Arctic-sourced moisture that is exported from the Arctic (row 4), and the change in the moisture from the rest of the globe that is imported into the Arctic (row 5), giving an estimate of the change in the contribution of locally sourced moisture to Arctic *P* (row 6).

	DJF	MAM	JJA	SON
Total Arctic ΔP	0.11	0.07	0.09	0.16
Total Arctic ΔE	0.08	0.03	0.01	0.07
Change in net moisture transport into Arctic	0.03	0.04	0.08	0.09
Arctic-sourced <i>E</i> to rest of globe (moisture exported from Arctic)	0.03	0.01	0.00	0.02
Rest of globe-sourced <i>E</i> to Arctic (remote contribution to Arctic <i>P</i>)	0.06	0.05	0.08	0.11
Arctic-sourced <i>E</i> to Arctic (local contribution to Arctic <i>P</i>)	0.05	0.02	0.01	0.05

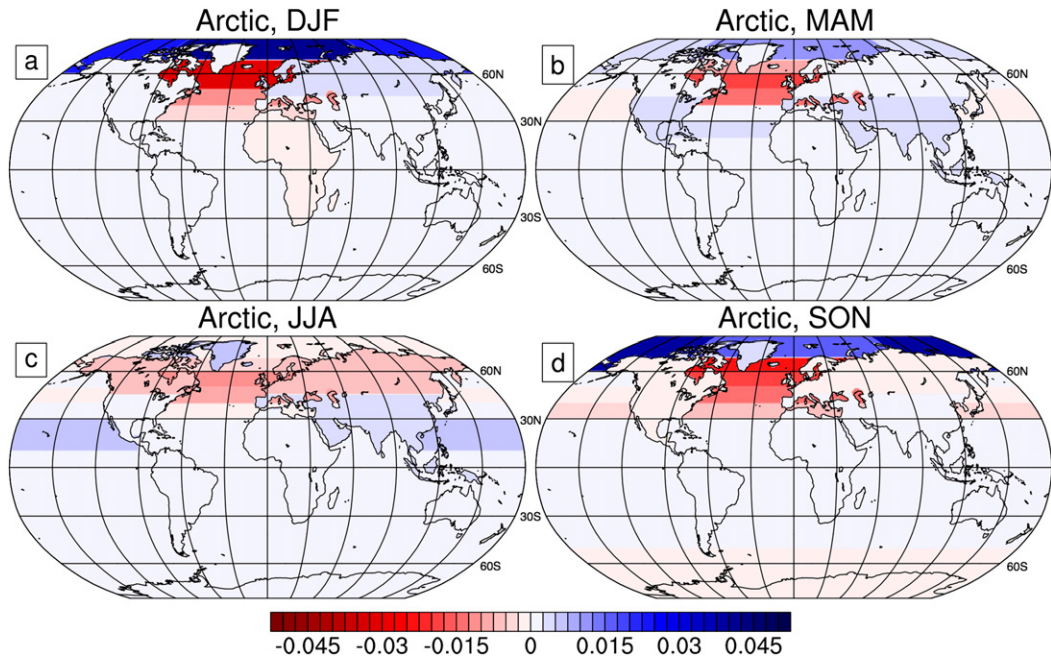


FIG. 5. Difference in the fractional moisture contribution of each tagged region to the Arctic precipitation between the CO₂-doubling and preindustrial control runs. Shown for (a) DJF, (b) MAM, (c) JJA, and (d) SON.

For the Arctic (Fig. 5; Table 3), local moisture source regions make up a greater fraction of the precipitation in winter (DJF) and fall (SON), particularly north of 70°N (Figs. 5a,d). On the other hand, the North Atlantic moisture source region, which contributes a large

fraction of the total Arctic precipitation the mean state, contributes a smaller fraction over all seasons; this is likely due to smaller surface temperature increases over the North Atlantic compared to the rest of the globe, which tends to moderate evaporation increases over this

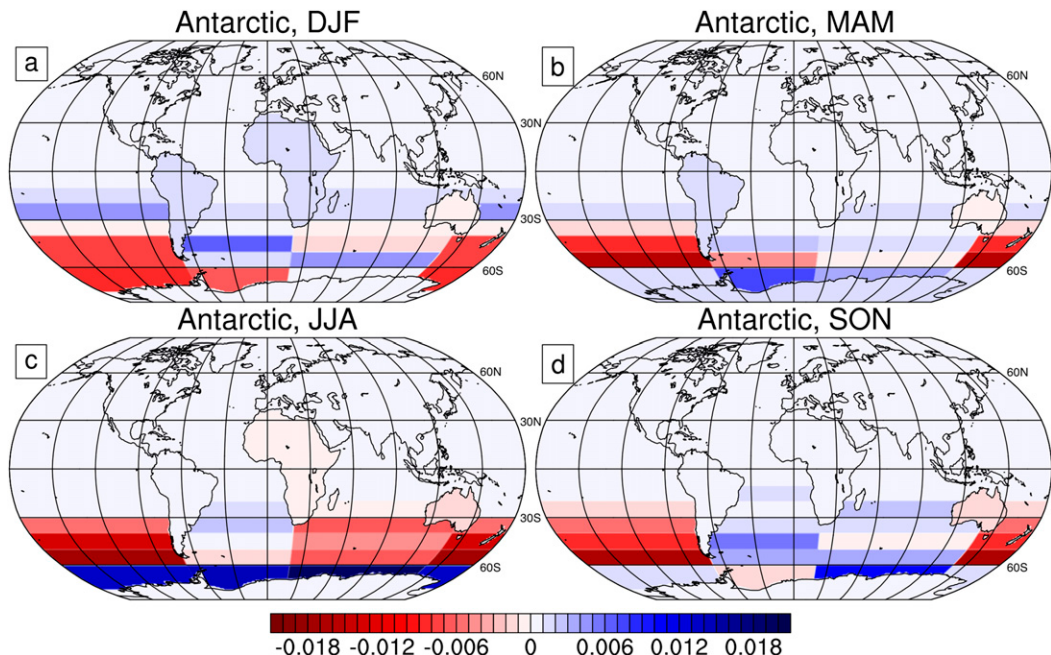


FIG. 6. As in Fig. 5, but for the Antarctic.

TABLE 3. Source regions of Arctic precipitation in the control and $2 \times \text{CO}_2$ runs in boreal winter (DJF) and summer (JJA). Quantities are given as an evaporative contribution (mm day^{-1}) with respect to the source region and as a percentage contribution to the total Arctic precipitation.

Tagged region	Control (mm day^{-1})	Control (%)	$2 \times \text{CO}_2$ (mm day^{-1})	$2 \times \text{CO}_2$ (%)
	DJF/JJA	DJF/JJA	DJF/JJA	DJF/JJA
Atlantic, 70°–90°N	0.48/0.15	10.6/3.8	0.82/0.18	14.6/3.7
Atlantic, 60°–70°N	1.59/0.32	23.1/5.4	1.70/0.36	20.0/5.1
Atlantic, 50°–60°N	0.96/0.28	19.6/6.6	0.99/0.28	16.4/5.5
Atlantic, 40°–50°N	0.40/0.17	11.0/5.2	0.44/0.17	9.7/4.3
Atlantic, 30°–40°N	0.23/0.12	7.9/4.6	0.27/0.14	7.4/4.4
Atlantic, 20°–30°N	0.10/0.11	3.3/4.3	0.12/0.13	3.4/4.5
Pacific, 60°–90°N	0.03/0.09	0.7/2.6	0.16/0.10	3.1/2.4
Pacific, 50°–60°N	0.15/0.06	3.4/1.7	0.19/0.08	3.5/1.7
Pacific, 40°–50°N	0.14/0.06	4.7/2.2	0.17/0.07	4.8/2.2
Pacific, 30°–40°N	0.11/0.08	4.8/4.0	0.15/0.10	5.0/4.0
Pacific, 20°–30°N	0.05/0.07	3.0/4.6	0.07/0.09	3.1/5.2
Pacific, 10°–20°N	0.02/0.03	1.0/2.0	0.02/0.04	1.1/2.6
Greenland	0.03/0.15	0.0/2.2	0.05/0.23	1.0/2.9
Eurasia, north of 45°N	0.02/0.20	1.0/21.6	0.03/0.23	1.9/21.1
Eurasia, south of 45°N	0.01/0.03	1.2/3.8	0.01/0.04	1.1/4.1
North America, north of 45°N	0.01/0.31	1.0/15.9	0.02/0.36	1.0/15.1
North America, south of 45°N	0.03/0.14	1.2/5.6	0.05/0.16	1.3/5.7

region (IPCC 2013). In summer (JJA; Fig. 5c), proximal moisture source regions contribute a smaller fraction of the precipitation (particularly over the Arctic itself, North Atlantic, northern Eurasia, and northern North America), and more distant moisture source regions contribute a greater fraction of the precipitation (southern Eurasia and subtropical Pacific). Overall, these results show that Arctic moisture source provenance

becomes more local in winter (DJF) and more distant in summer (JJA).

Over the Antarctic, we find similar changes in moisture source provenance (Fig. 6; Table 4). In winter (JJA; Fig. 6c), local moisture sources, particularly ocean source regions south of 60°S, contribute a greater fraction of the polar precipitation; at the same time, remote moisture source regions contribute a smaller fraction of

TABLE 4. As in Table 3, but for the Antarctic precipitation.

Tagged region	Control (mm day^{-1})	Control (%)	$2 \times \text{CO}_2$ (mm day^{-1})	$2 \times \text{CO}_2$ (%)
	DJF/JJA	DJF/JJA	DJF/JJA	DJF/JJA
Atlantic, 60°–90°S	0.25/0.11	3.5/1.3	0.25/0.29	2.8/2.7
Atlantic, 50°–60°S	0.24/0.34	4.1/5.0	0.31/0.43	4.3/4.8
Atlantic, 40°–50°S	0.31/0.35	6.3/6.0	0.42/0.46	6.9/6.1
Atlantic, 30°–40°S	0.18/0.23	3.4/3.6	0.24/0.31	3.5/3.8
Atlantic, 20°–30°S	0.09/0.09	1.8/1.4	0.13/0.12	2.0/1.5
Atlantic, 10°–20°S	0.04/0.02	0.6/0.3	0.06/0.04	0.7/0.4
Pacific, 60°–90°S	0.33/0.37	8.2/7.9	0.37/0.56	7.4/9.2
Pacific, 50°–60°S	0.37/0.49	10.7/12.0	0.43/0.54	10.0/10.2
Pacific, 40°–50°S	0.35/0.42	12.1/12.2	0.41/0.48	11.4/10.9
Pacific, 30°–40°S	0.20/0.31	7.1/8.9	0.25/0.37	7.0/8.4
Pacific, 20°–30°S	0.08/0.12	3.3/4.2	0.11/0.15	3.8/4.2
Pacific, 10°–20°S	0.03/0.04	1.1/1.3	0.04/0.05	1.4/1.4
Indian Ocean, 70°–90°S	0.28/0.25	3.3/2.5	0.35/0.57	3.3/4.4
Indian Ocean, 60°–70°S	0.32/0.48	7.4/9.4	0.42/0.58	7.8/8.8
Indian Ocean, 50°–60°S	0.36/0.41	10.3/9.9	0.44/0.50	10.2/9.5
Indian Ocean, 40°–50°S	0.22/0.33	5.9/7.6	0.27/0.40	5.9/7.0
Indian Ocean, 30°–40°S	0.09/0.12	2.2/2.5	0.12/0.15	2.4/2.4
Indian Ocean, 20°–30°S	0.02/0.02	0.5/0.5	0.03/0.03	0.7/0.6
Antarctica	0.05/0.01	1.9/0.2	0.07/0.01	2.0/0.3
Australia	0.08/0.06	1.7/1.0	0.10/0.06	1.6/0.9
South America	0.05/0.03	2.4/1.1	0.07/0.04	2.6/1.2

the polar precipitation, particularly over the midlatitude Pacific. In summer (DJF; Fig. 6a), on the other hand, more remote moisture source regions contribute a greater fraction of the polar precipitation, particularly the subtropical Pacific between 30° and 20°S; more proximal moisture source regions, particularly the midlatitude Pacific, contribute a smaller fraction of the polar precipitation.

We find that for both the Arctic and Antarctic, the summer season (JJA for the Arctic, DJF for the Antarctic) changes are dominated by an increase in remotely sourced moisture that originates from farther equatorward (approximately 3° latitude more equatorward over the Arctic and 1.5° latitude more equatorward over the Antarctic), while the winter season (DJF for the Arctic and JJA for the Antarctic) changes are dominated by an increase in locally sourced moisture, particularly from polar ocean regions. This suggests that similar seasonal processes drive the response to CO₂ doubling in both hemispheres. We will consider these mechanisms of seasonal polar hydrologic cycle change in the following section.

c. Mechanisms of moisture source change

To understand the mechanisms driving polar hydrologic cycle change, we use the matrix operator framework developed in Singh et al. (2016b) and apply it to the polar regions. As described in Singh et al. (2016b), the change in the precipitation $\Delta\mathbf{P}$ may be written as

$$\Delta\mathbf{P} = (\Delta\mathbf{M})\mathbf{E} + \mathbf{M}(\Delta\mathbf{E}), \quad (2)$$

where \mathbf{M} is the transport matrix, \mathbf{E} is the evaporation vector, and the Δ operator signifies the change between the CO₂-doubling experiment and the control. In Eq. (2), total $\Delta\mathbf{P}$ has been decomposed partly as a result of changes in transport $(\Delta\mathbf{M})\mathbf{E}$ and partly as a result of changes in evaporation $\mathbf{M}(\Delta\mathbf{E})$.

Since the polar precipitation change can be decomposed into parts as a result of changes in locally sourced and remotely sourced moisture, each of these local and remote components can be further separated into parts as a result of transport and evaporation changes:

$$\begin{aligned} (\Delta\mathbf{P})_{\text{local}} + (\Delta\mathbf{P})_{\text{remote}} &= [(\Delta\mathbf{M})\mathbf{E}]_{\text{local}} + [(\Delta\mathbf{M})\mathbf{E}]_{\text{remote}} \\ &\quad + [\mathbf{M}(\Delta\mathbf{E})]_{\text{local}} + [\mathbf{M}(\Delta\mathbf{E})]_{\text{remote}}. \end{aligned} \quad (3)$$

We show the components of this decomposition in Fig. 7, which reveals similarities between the mechanisms driving the hydrologic cycle response in the NH and SH polar regions. In general, the polar precipitation change driven by changes in evaporation is largest in

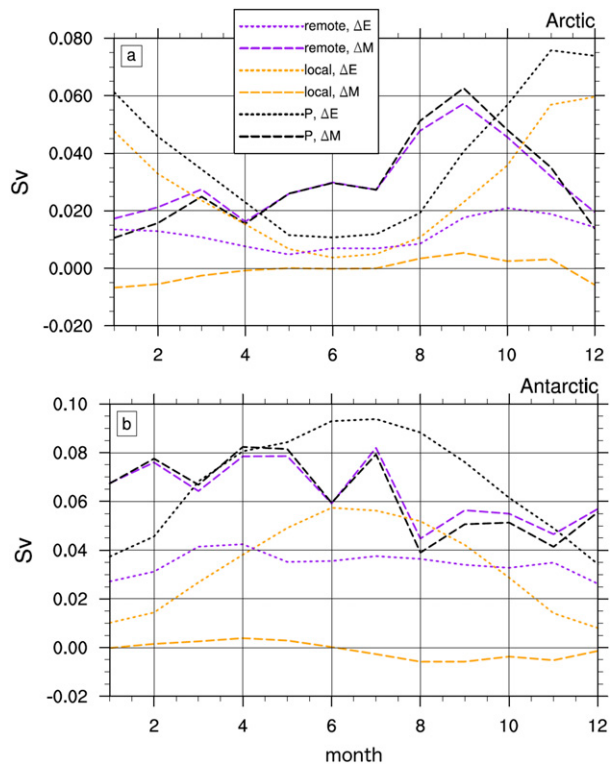


FIG. 7. Decomposition of the monthly change in total polar precipitation (black lines) and its local (yellow lines) and remote (purple lines) components into parts due to $\Delta\mathbf{E}$ (dotted lines) and $\Delta\mathbf{M}$ (dashed lines), as in Eq. (3), shown for the (a) Arctic and (b) Antarctic.

winter and smallest in summer (Fig. 7, black dotted lines). In both hemispheres, the strong seasonality of the evaporation-driven polar precipitation change (black dotted lines) is due to changes in the local contribution (yellow dotted lines); the evaporation-driven remote contribution, in contrast, is relatively constant year-round (purple dotted lines).

Changes in polar precipitation that are driven by changes in transport peak in fall in both hemispheres (Fig. 7, black dashed lines). This transport-driven precipitation change is smallest in the Arctic in winter but is smallest in the Antarctic in spring, suggesting subtle seasonal differences between the hemispheres. This transport-driven precipitation change (black dashed lines) is dominated by remotely sourced precipitation (purple dashed lines). The transport-driven change in the locally sourced precipitation is small year-round (yellow dashed line); this term tends to modestly increase the precipitation in fall but tends to decrease it in late winter and early spring.

In both hemispheres, we find that evaporation-driven precipitation changes dominate in winter, while

transport-driven changes dominate in late summer and early fall. We now consider the mechanisms of polar precipitation change in greater detail from the viewpoint of moisture source regions. From a source–receptor perspective, we can write the portion of the polar precipitation sourced from j , $P_{j,\text{polar}}$, as the fraction of the evaporation from region j , E_j , that is exported from j and directed toward the polar cap:

$$P_{j,\text{polar}} = f_{\text{polar},j} e_j E_j, \quad (4)$$

where e_j is the fraction of moisture evaporated from j that is not precipitated over that region (i.e., is exported) and $f_{\text{polar},j}$ is the fraction of this exported moisture that precipitates over the polar cap. Similarly, the local contribution to the precipitation can be written as

$$P_{\text{local,polar}} = (1 - e_{\text{local}}) E_{\text{local}}, \quad (5)$$

where E_{local} is the local evaporation and $1 - e_{\text{local}}$ is the fraction of the locally evaporated moisture that precipitates locally. From this, it follows that the total precipitation over the polar cap P_{polar} is the sum of these remote contributions to the precipitation over all j [Eq. (4)] and the local contribution [Eq. (5)]:

$$P_{\text{polar}} = \sum_j f_{\text{polar},j} e_j E_j + (1 - e_{\text{local}}) E_{\text{local}}. \quad (6)$$

The decomposition of the polar precipitation [Eq. (6)] can be written as follows:

$$\begin{aligned} \Delta P_{\text{polar}} \approx & \sum_j [\Delta(f_{\text{polar},j}) e_j E_j] + \sum_j [f_{\text{polar},j} \Delta(e_j) E_j] \\ & - \Delta(e_{\text{local}}) E_{\text{local}} + \sum_j [f_{\text{polar},j} e_j \Delta(E_j)] \\ & + (1 - e_{\text{local}}) \Delta(E_{\text{local}}), \end{aligned} \quad (7)$$

where terms have been grouped as those resulting from

- 1) transport direction changes—the change in the relative fraction of exported moisture from j that is directed toward the pole (rather than elsewhere);
- 2) export efficiency changes—the change in fraction of moisture evaporated from each j and the polar cap that is exported; and
- 3) evaporation changes—the change in surface evaporation in j and the polar cap.

Taken together, terms 1 and 2 signify changes in how moisture is transported (with evaporation held constant), while term 3 accounts for changes in evaporation (with transport held constant). As noted in Singh et al. (2016a), changes in evaporation and changes in transport in the matrix operator framework should not be

construed to be equivalent to Eulerian changes in thermodynamics and changes in dynamics, respectively. From an Eulerian perspective, much of the change in polar precipitation can be attributed to increased atmospheric moisture (i.e., thermodynamics), which tends to intensify evaporation minus precipitation ($E - P$) and moisten the high latitudes. The source–receptor analysis that we present here offers an alternative framework for attributing these same hydrologic cycle changes.

In Figs. 8 and 9, we consider whether changes in evaporation or changes in transport drive the seasonal hydrologic cycle response to CO₂ doubling. The winter season (DJF) change in moisture source provenance for the Arctic is shown in Fig. 8a and reveals that increased winter precipitation over the polar cap strongly depends on the increase in locally sourced moisture, with smaller increases in remotely sourced moisture from the Atlantic and Pacific midlatitudes and North America. The increase in locally sourced moisture is driven by increased evaporation (Fig. 8d), while changes in moisture transport, through increased export, tend to counteract the effect of increased local evaporation by exporting more of this moisture away from the Arctic (Fig. 8c). Overall, increased evaporation over the polar cap drives a large fraction of the increased wintertime precipitation over the Arctic. On the other hand, changes in moisture transport that direct a greater fraction of moisture toward the pole tend to modestly increase polar precipitation sourced from the midlatitudes (Fig. 8b), though this change is much smaller in magnitude than that caused by local evaporation. The North Atlantic source region (between 50° and 60°N) is somewhat anomalous, in that changes in transport that tend to divert moisture away from the polar cap dominate (Fig. 8b).

In summer (JJA), on the other hand, increased Arctic precipitation is less dependent on locally sourced evaporation and more dependent on moisture evaporated from distant source regions (Fig. 8e). Much of this change is due to changes in moisture transport, including greater diversion of moisture sourced from the subtropical and midlatitude oceans to the polar cap (Fig. 8f), and greater export of moisture from northern North America, northern Eurasia, and the North Atlantic (Fig. 8g). Increased evaporation, on the other hand, plays a much smaller role than in winter (cf. Fig. 8h to Fig. 8d), mainly increasing precipitation sourced from the polar cap itself and northern North America. Surprisingly, precipitation sourced from the North Atlantic (between 40° and 60°N) decreases (Fig. 8e), as a result of less evaporation from this region (Fig. 8h), likely caused by cooler summer SSTs over the North Atlantic that are common to many GCMs (IPCC 2013).

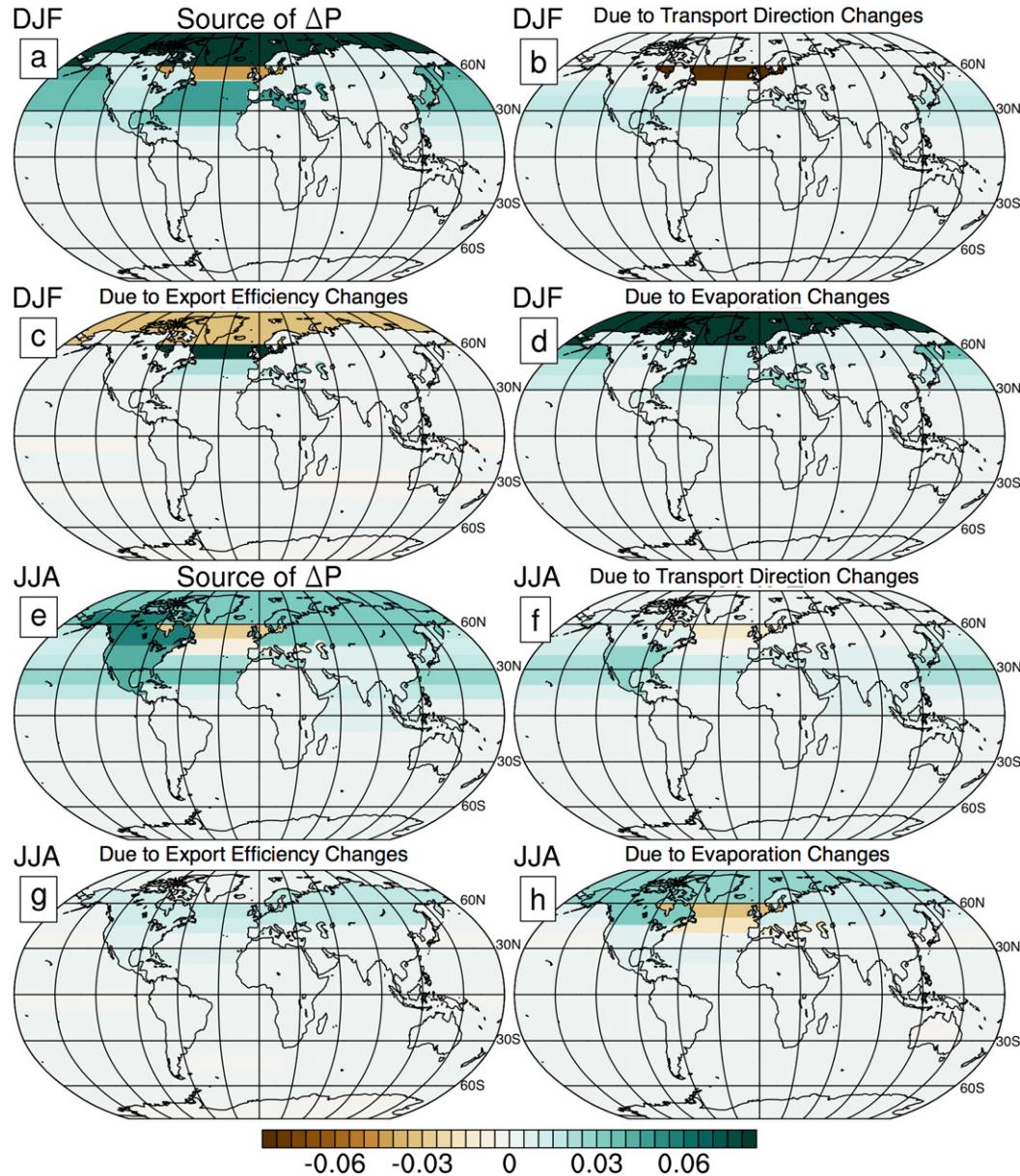


FIG. 8. Attribution of the change in moisture contribution from each tagged region to the Arctic precipitation (computed in mm day^{-1} using the area of the source region) between the CO_2 -doubling and preindustrial control runs: (a),(e) total change in Arctic precipitation moisture sources; (b),(f) change in source of Arctic P as a result of changes in transport direction (i.e., changes in the partitioning of remotely sourced moisture between sink regions $\Delta f_{\text{polar},j}$); (c),(g) change in source of Arctic P as a result of changes in export efficiency (i.e., changes in the moisture export fraction, Δe_j , and Δe_{polar}); and (d),(h) change in source of Arctic P as a result of changes in evaporation ΔE . Shown for (a)–(d) DJF and (e)–(h) JJA.

Figure 9 reveals that mechanisms driving seasonal changes in polar moisture source provenance are similar between the Arctic and Antarctic. In the Antarctic, changes in summertime (DJF) precipitation are dominated by increased moisture sourced from the mid-latitude and subtropical oceans (Fig. 9a). Over half of

this response is due to changes in moisture transport, which tend to divert moisture evaporated from more distant regions, including the midlatitudes and subtropics, toward the polar cap (Fig. 9b; cf. the Arctic, Fig. 8f); changes caused by increased moisture export are small (Fig. 9c). On the other hand, increased

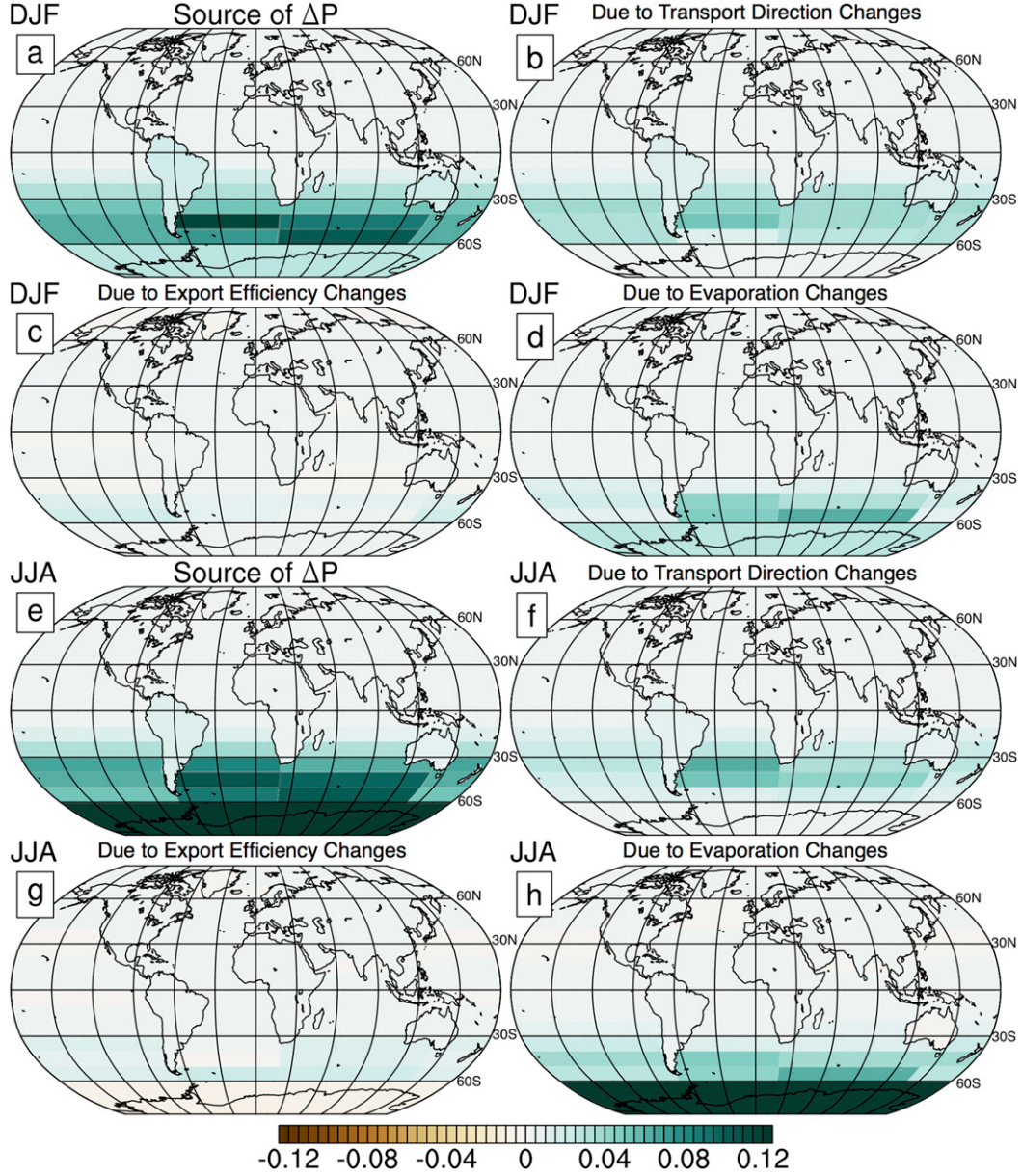


FIG. 9. As in Fig. 8, but for the Antarctic.

evaporation tends to increase precipitation sourced locally and from more proximal sources, particularly from the Indian Ocean Basin and the Atlantic basin between 40° and 60°S (Fig. 9d; cf. the Arctic, Fig. 8h).

In Antarctic winter (JJA), as in Arctic winter, a large increase in precipitation from local moisture source regions is evident (Fig. 9e; cf. Fig. 8a). Most of this increase in locally sourced moisture is due to increased local and proximal evaporation, similar to that seen in the Arctic (Fig. 9h; cf. to the Arctic, Fig. 8d). Modest changes in transport are also evident, as moisture from more

remote midlatitude and subtropical ocean regions is preferentially directed toward the pole (Fig. 9f; cf. to the Arctic, Fig. 8b). As for the Arctic, changes in moisture export tend to decrease the local contribution to the precipitation while also slightly increasing the remote contribution (Fig. 9g; cf. the Arctic, Fig. 8c).

Overall, Figs. 8 and 9 show that winter and summer mechanisms of polar hydrologic cycle changes are distinct. While increased local evaporation dominates in winter, changes in both transport and evaporation (local and remote) are important in summer. In Singh et al.

(2016a), we showed that from a global perspective, changes in moisture transport with CO₂ doubling tend to increase the distance between moisture source and sink regions. For the polar regions, this assessment is true in summer, but it does not account for the increase in locally sourced moisture in winter. We consider why evaporation increases so strongly over the polar oceans in winter in the following section.

THE ROLE OF SEA ICE RETREAT IN WINTER

Many studies show that retreating sea ice cover will expose more open ocean to the atmosphere, thereby enhancing turbulent surface sensible and latent heat fluxes (Screen and Simmonds 2010). In our experiments, we find that turbulent latent heat fluxes are greatly enhanced over areas of sea ice retreat in both hemispheres only in the winter season (DJF for the Arctic, JJA for the Antarctic), not summer (JJA for the Arctic, DJF for the Antarctic; cf. Figs. 10a,d with Figs. 10b,c). In the Arctic, this coincident decrease in winter sea ice concentration and increase in surface latent heat flux is mostly found in the Barents Sea, the Greenland–Iceland Strait, the Chuckchi Sea, and the Bering Sea (Fig. 10a); in the Antarctic, these regions of sea ice retreat and latent heat flux intensification are found around the entire Antarctic continent (Fig. 10d). In both hemispheres, summer latent heat fluxes are not enhanced over areas of sea ice retreat (Figs. 10b,c) despite substantial changes in summer sea ice cover.

To understand why surface evaporation increases so substantially over areas of sea ice retreat in winter in both hemispheres (DJF for the Arctic, JJA for the Antarctic), we consider the bulk formula for surface E , which can be written as

$$E = \rho C_{\text{Ea}} U_{10} [q_s(T_s) - q_a], \quad (8)$$

where C_{Ea} is the bulk transfer coefficient (used to parameterize the efficiency of turbulent surface processes), U_{10} is the 10-m surface wind speed, $q_s(T_s)$ is the (temperature dependent) saturation specific humidity at the surface, and q_a is the atmospheric specific humidity above the surface (Peixoto and Oort 1992). We emphasize that changes in surface evaporation involve changes in both thermodynamics (temperature and humidity) and dynamics (boundary layer winds); therefore, changes in evaporation should be not construed as driven solely by either thermodynamics or dynamics but rather a combination of the two, depending on the relevant factors involved.

We find that both thermodynamics and dynamics favor increased surface evaporation over areas of sea retreat in winter: an enhancement of the specific humidity

gradient between the surface and overlying air ($q_s - q_a$; Figs. 11a,d) and enhancement of the surface winds (U_{10} ; Figs. 12a,d) act together to increase latent heat fluxes. These drivers of increased evaporation over areas of sea ice retreat in winter are remarkably similar between the Arctic and Antarctic.

In summer (JJA for the Arctic, DJF for the Antarctic), on the other hand, latent heat fluxes over areas of sea ice retreat remain unchanged in both hemispheres because these same factors do not favor increased evaporation: surface temperatures remain constrained near the melting point of ice, rendering little change in the specific humidity gradient at the surface (Figs. 11b,c); and surface winds increase only modestly over areas of sea ice retreat (Figs. 12b,c) compared to winter.

4. Discussion and conclusions

Over the last several decades, the Arctic and Antarctic have displayed very different transient sensitivities to greenhouse gas emissions and other anthropogenic forcings [for a review, see Turner et al. (2007)]. Despite these very different responses, we find that from a source–receptor perspective, the seasonal hydrologic cycle response to CO₂ doubling in the CESM is very similar in the Arctic and Antarctic.

During all seasons, polar precipitation increases in the CESM with CO₂ doubling. This increase is due to both an increase in the convergence of remotely sourced moisture (the remote contribution) and an increase in precipitation sourced from locally evaporated moisture (the local contribution). We have used numerical water tracers in the CESM to demonstrate that the increase in the remote contribution significantly exceeds the increase in the local contribution in the Arctic and Antarctic in the annual mean and over nearly all seasons (with the exception being in the Arctic in winter). This conclusion is at odds with the CESM result obtained using budget methods (recall Table 2). Since budget methods do not account for the export of locally evaporated moisture away from the polar regions, we suggest that studies that rely on budget methods for evaluating polar moisture source provenance (such as multimodel intercomparison studies) could minimize biases in their assessments of local and remote contributions by applying a correction factor to account for this local moisture export.

Over their respective summer seasons, the CESM polar hydrologic cycle response to CO₂ doubling in both the NH and SH is due to changes in both moisture transport and evaporation: evaporation increases in remote regions and a greater fraction of this remote moisture is directed toward the pole. With CO₂

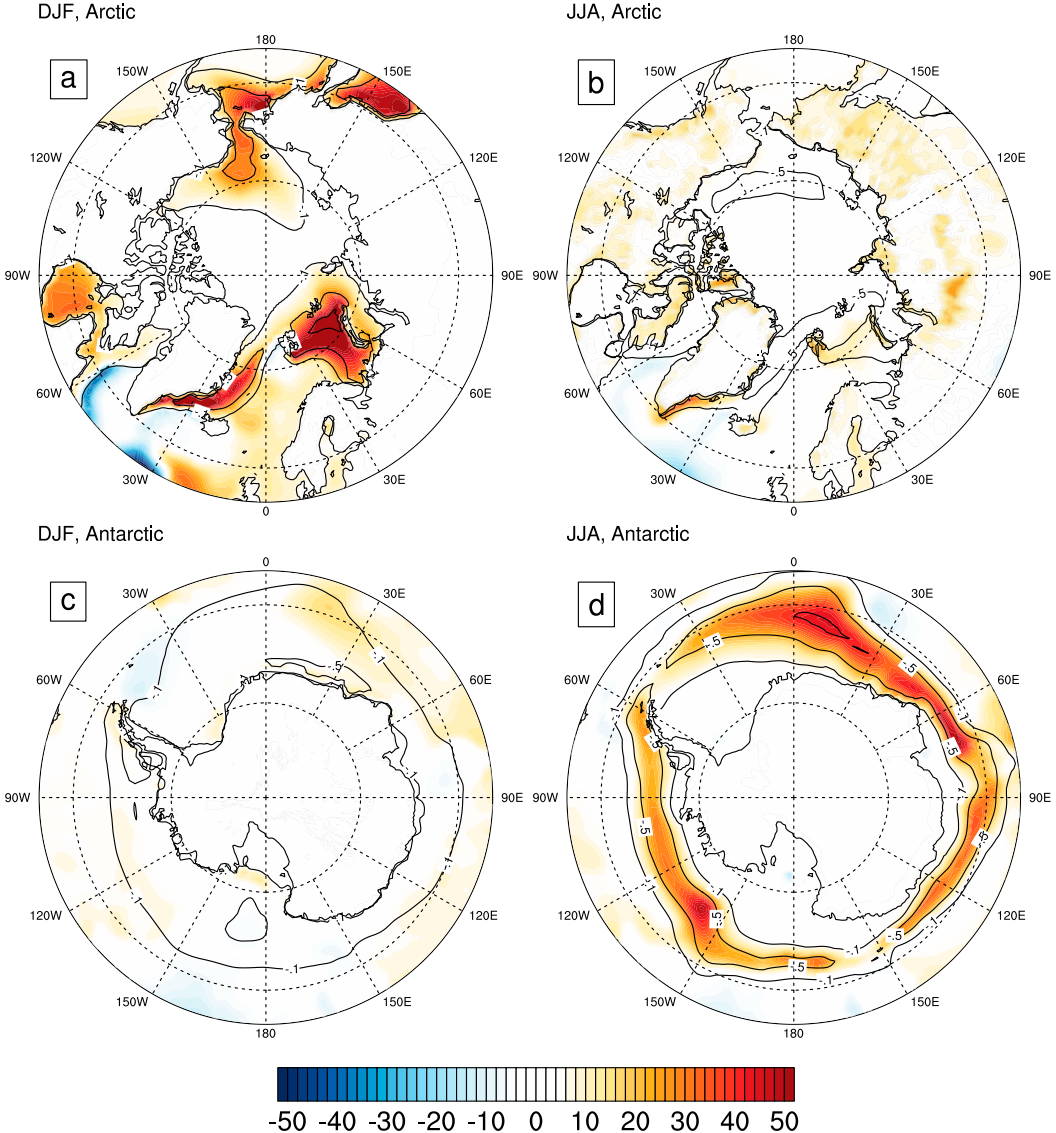


FIG. 10. Change in sea ice fraction (contours at 0.1, 0.5, and 0.9) and surface latent heat flux (colors; W m^{-2}) between the CO_2 -doubling and preindustrial control runs. Shown for the (a),(b) Arctic and (c),(d) Antarctic for (a),(c) DJF and (b),(d) JJA.

doubling, precipitation sources change such that remote sources are favored over local ones and more remote source regions are favored over less remote ones. As a result, the distance between moisture source and sink regions lengthens in summer, and equatorward moisture sources contribute a greater fraction of the polar precipitation than poleward ones. This summertime polar response to CO_2 -induced warming is consistent with the year-round response over the rest of the globe, namely, an increase in the moisture residence time and the moisture transport length scale (Singh et al. 2016a).

Over winter, however, our model exhibits a marked increase in polar evaporation over areas of sea ice retreat,

which enhances the relative contribution of local moisture source regions and effectively decreases the distance between moisture sources and sinks. This large increase in local evaporation in winter with CO_2 doubling is partly due to the different thermodynamic impact of sea ice loss between the winter and summer seasons: in summer, surface temperatures are locked near the melting point and the saturation specific humidity near the surface remains unchanged; in winter, in contrast, the climatological air temperature above sea ice is very cold and the surface temperature (and saturation specific humidity) increases considerably in regions where sea ice gives way to open ocean, driving large evaporation increases.

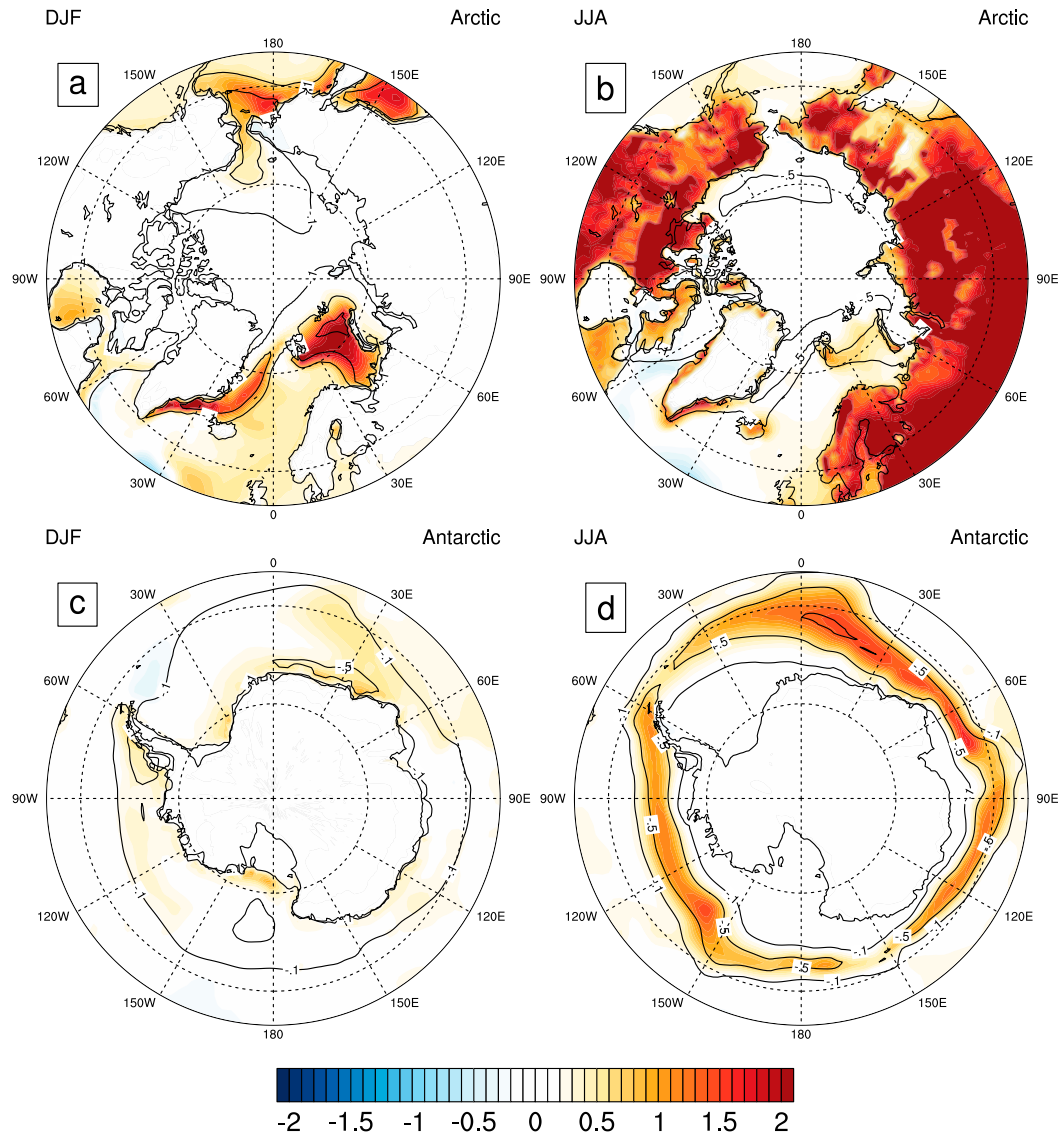
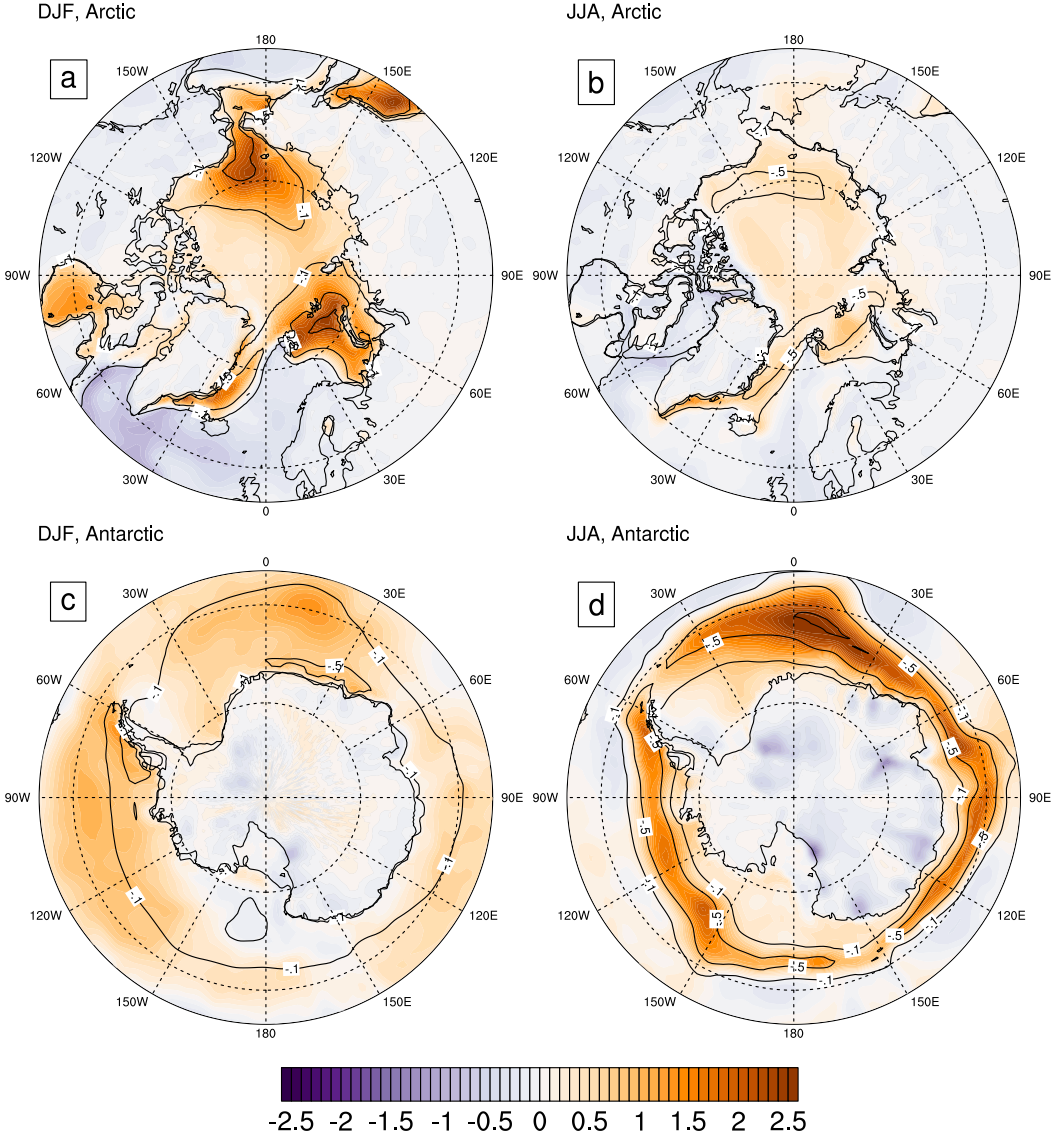


FIG. 11. Change in the gradient between the surface saturation specific humidity and the atmospheric specific humidity above the surface [$(q_s - q_a)$, colors; g kg^{-1}] between the CO₂-doubling and preindustrial control runs, shown with the change in sea ice fraction (contours at 0.1, 0.5, and 0.9). Given for the (a),(b) Arctic and (c),(d) Antarctic in (a),(c) DJF and (b),(d) JJA.

We have shown that the polar hydrologic cycle response to CO₂-induced warming is strongly seasonal in the CESM. This is contrary to the hydrologic cycle response over the rest of the globe, which can be described well by assessing the annual mean response (Singh et al. 2016a). In the mean state, moreover, we have shown moisture source provenance is strongly seasonal only over the Arctic, where the predominant moisture source region shifts between the North Atlantic in winter and the Eurasian and North American continents in summer; no comparable ocean-to-land shift in moisture source provenance is seen in the Antarctic, likely resulting from the presence of the surrounding circumpolar ocean,

making Antarctic moisture source regions relatively constant year-round. Therefore, the seasonality of the mean state is not sufficient to explain the strong seasonality of the polar precipitation response.

Why is there Arctic–Antarctic parity in the polar hydrologic cycle response to CO₂-induced warming in the CESM? This is particularly surprising given the different mean state hydrologic cycles in the Arctic and Antarctic. We argue that Arctic–Antarctic parity in changes in polar moisture source provenance with CO₂ doubling is due to the fact that the relevant mechanistic processes that drive the response to CO₂ doubling do not differ substantially between the two hemispheres. In

FIG. 12. As in Fig. 11, but for U_{10} (colors; m s^{-1}).

particular, sea ice loss with warming is common in both hemispheres in most GCMs (IPCC 2013), albeit not in the Antarctic in the present day; furthermore, fundamental changes in moisture transport, particularly the lengthening of moisture transport pathways, are evident globally and are also manifested in the polar regions. This robust response in both hemispheres suggests that these seasonally distinct polar hydrologic cycle changes are common to climate states similar to that of the present day. Arctic–Antarctic parity suggests that the processes responsible for these similarities are fundamental to the climate system.

We have shown that the CESM polar hydrologic cycle differs from that of the rest of the globe, in that the presence of sea ice renders a distinct winter season

hydrologic cycle response. An important implication of this result lies in the interpretation of paleo-proxy isotope records from ice cores: given that the polar hydrologic cycle response to CO_2 doubling is tightly coupled to a nonlinear process, the winter retreat of sea ice, interpreting such proxy records using ad hoc back-of-the-envelope analysis methods should be undertaken cautiously. While this is true for any isotopic record in which the climate state differs significantly from that of the present as a result of changes in moisture transport, it is especially true of the polar regions where the retreat of sea ice adds an additional layer of complexity to the response.

We conclude by emphasizing a major caveat of the results described in this work. We have made our

conclusions by assessing the hydrologic cycle response to CO₂ doubling in a single GCM. Since there are uncertainties associated with GCM representations of the hydrologic cycle, it is likely that some of the results presented here are peculiar to the CESM. Sea ice biases in the CESM, for example, may affect the magnitude and location of polar precipitation change because of local moisture sources. Further analyses of other state-of-the-art GCMs and real-world observations will be required to confirm that these results are robust. Nevertheless, our analysis offers a compelling case that there are similarities between the Arctic and Antarctic in their hydrologic cycle responses to CO₂ doubling, and suggests that there may be other robust similarities between the two polar regions in how they respond to anthropogenic CO₂ emissions.

Acknowledgments. The authors are indebted to Jesse Nusbaumer and David Noone for their development of the tagged version of CAM5.0, and to NCAR's Computational and Information Systems Laboratory for use of Yellowstone supercomputing facilities (<http://n2t.net/ark:/85065/d7wd3xhc>), sponsored by the NSF. HKAS is grateful for use of facilities and funding from the DOE Office of Science through the Pacific Northwest National Laboratory's Linus Pauling Distinguished Postdoctoral Fellowship. AD was funded by a SEED grant from the Applied Physics Laboratory at the University of Washington. This work was also supported in part by the Regional and Global Climate Modeling Program of the Office of Biological and Environmental Research in the U.S. Department of Energy's Office of Science as a contribution to the HiLAT project. The Pacific Northwest National Laboratory is operated for the U.S. Department of Energy by Battelle Memorial Institute under Contract DE-AC05-76RL01830. The authors also wish to thank Harald Sodemann and two anonymous reviewers for helpful manuscript critiques.

REFERENCES

- Bengtsson, L., K. Hodges, S. Koumoutsaris, M. Zahn, and N. Keenlyside, 2011: The changing atmospheric water cycle in Polar Regions in a warmer climate. *Tellus*, **63A**, 907–920, doi:[10.1111/j.1600-0870.2011.00534.x](https://doi.org/10.1111/j.1600-0870.2011.00534.x).
- Bintanja, R., and F. Selten, 2014: Future increases in Arctic precipitation linked to local evaporation and sea-ice retreat. *Nature*, **509**, 479–482, doi:[10.1038/nature13259](https://doi.org/10.1038/nature13259).
- Bosilovich, M., and S. Schubert, 2002: Water vapor tracers as diagnostics of the regional hydrologic cycle. *J. Hydrometeor.*, **3**, 149–165, doi:[10.1175/1525-7541\(2002\)003<0149:WVTA>2.0.CO;2](https://doi.org/10.1175/1525-7541(2002)003<0149:WVTA>2.0.CO;2).
- Boyer, T., S. Levitus, J. Antonov, R. Locarnini, and H. Garcia, 2005: Linear trends in salinity for the World Ocean, 1955–1998. *Geophys. Res. Lett.*, **32**, L01604, doi:[10.1029/2004GL021791](https://doi.org/10.1029/2004GL021791).
- Caias, P., J. White, J. Jouzel, and R. Petit, 1995: The origin of present-day Antarctic precipitation from surface snow deuterium excess data. *J. Geophys. Res.*, **100**, 18 917–18 927, doi:[10.1029/95JD01169](https://doi.org/10.1029/95JD01169).
- Durack, P., and S. Wijffels, 2010: Fifty-year trends in global ocean salinities and their relationship to broad-scale warming. *J. Climate*, **23**, 4342–4362, doi:[10.1175/2010JCLI3377.1](https://doi.org/10.1175/2010JCLI3377.1).
- , —, and R. Matear, 2012: Ocean salinities reveal strong global water cycle intensification during 1950 to 2000. *Science*, **336**, 455–458, doi:[10.1126/science.1212222](https://doi.org/10.1126/science.1212222).
- Groves, D., and J. Francis, 2002: Variability of the Arctic atmospheric moisture budget from TOVS satellite data. *J. Geophys. Res.*, **107**, 4785, doi:[10.1029/2002JD002285](https://doi.org/10.1029/2002JD002285).
- Hartmann, D., 1994: *Global Physical Climatology*. International Geophysics Series, Vol. 56, Academic Press, 411 pp.
- Held, I., and B. Soden, 2006: Robust responses of the hydrological cycle to global warming. *J. Climate*, **19**, 5686–5699, doi:[10.1175/JCLI3990.1](https://doi.org/10.1175/JCLI3990.1).
- Helm, K., N. Bindoff, and J. Church, 2010: Changes in the global hydrological-cycle inferred from ocean salinity. *Geophys. Res. Lett.*, **37**, L18701, doi:[10.1029/2010GL044222](https://doi.org/10.1029/2010GL044222).
- Holland, M., and C. Bitz, 2003: Polar amplification of climate change in coupled models. *Climate Dyn.*, **21**, 221–232, doi:[10.1007/s00382-003-0332-6](https://doi.org/10.1007/s00382-003-0332-6).
- Hurrell, J., and Coauthors, 2013: The Community Earth System Model: A framework for collaborative research. *Bull. Amer. Meteor. Soc.*, **94**, 1339–1360, doi:[10.1175/BAMS-D-12-00121.1](https://doi.org/10.1175/BAMS-D-12-00121.1).
- Hwang, Y.-T., and D. Frierson, 2010: Increasing atmospheric poleward energy transport with global warming. *Geophys. Res. Lett.*, **37**, L24807, doi:[10.1029/2010GL045440](https://doi.org/10.1029/2010GL045440).
- IPCC, 2013: Summary for policymakers. *Climate Change 2013: The Physical Science Basis*, T. F. Stocker et al., Eds., Cambridge University Press, 3–29.
- Jakobson, E., and T. Vihma, 2010: Atmospheric moisture budget in the Arctic based on the ERA-40 reanalysis. *Int. J. Climatol.*, **30**, 2175–2194, doi:[10.1002/joc.2039](https://doi.org/10.1002/joc.2039).
- Johnsen, S., and J. White, 1989: The origin of Arctic precipitation under present and glacial conditions. *Tellus*, **41B**, 452–468, doi:[10.1111/j.1600-0889.1989.tb00321.x](https://doi.org/10.1111/j.1600-0889.1989.tb00321.x).
- Joussaume, S., R. Sadourny, and C. Vignal, 1986: Origin of precipitating water in a numerical simulation of July climate. *Ocean–Air Interact.*, **1**, 43–56.
- Koster, R., J. Jouzel, R. Suozzo, G. Russell, W. Broecker, D. Rind, and P. Eagleson, 1986: Global sources of local precipitation as determined by the NASA/GISS GCM. *Geophys. Res. Lett.*, **13**, 121–124, doi:[10.1029/GL013i002p00121](https://doi.org/10.1029/GL013i002p00121).
- , —, —, and —, 1992: Origin of July Antarctic precipitation and its influence on deuterium content: A GCM analysis. *Climate Dyn.*, **7**, 195–203, doi:[10.1007/BF00206861](https://doi.org/10.1007/BF00206861).
- Levitus, S., and Coauthors, 2013: The World Ocean Database. *Data Sci. J.*, **12**, 229–234, doi:[10.2481/dsj.wds-041](https://doi.org/10.2481/dsj.wds-041).
- Manabe, S., and R. Stouffer, 1994: Multiple-century response of a coupled ocean–atmosphere model to an increase of atmospheric carbon dioxide. *J. Climate*, **7**, 5–23, doi:[10.1175/1520-0442\(1994\)007<0005:MCROAC>2.0.CO;2](https://doi.org/10.1175/1520-0442(1994)007<0005:MCROAC>2.0.CO;2).
- Neale, R., and Coauthors, 2012: Description of NCAR Community Atmosphere Model (CAM 5.0). NCAR Tech. Note NCAR/TN-486+STR, 274 pp.
- Noone, D., and I. Simmonds, 2002: Annular variations in moisture transport mechanisms and the abundance of δ¹⁸O in Antarctic snow. *J. Geophys. Res.*, **107**, 4742, doi:[10.1029/2002JD002262](https://doi.org/10.1029/2002JD002262).
- Oshima, K., and K. Yamazaki, 2004: Seasonal variation of moisture transport in polar regions and the relation with the annular modes. *Polar Meteor. Glaciol.*, **18**, 30–53.

- Overland, J., and P. Turet, 1994: Variability of atmospheric energy flux across 70°N computed from the GFDL data set. *The Polar Oceans and Their Role in Shaping the Global Environment, Geophys. Monogr.*, Vol. 85, Amer. Geophys. Union, 313–325.
- Peixoto, J., and A. Oort, 1992: *Physics of Climate*. American Institute of Physics, 520 pp.
- Peterson, B., R. Holmes, J. McClelland, C. Vorosmarty, R. Lammers, A. Shiklomanov, I. Shiklomanov, and S. Rahmstorf, 2002: Increasing river discharge to the Arctic Ocean. *Science*, **298**, 2171–2173, doi:[10.1126/science.1077445](https://doi.org/10.1126/science.1077445).
- , J. McClelland, R. Curry, R. Holmes, J. Walsh, and K. Aagard, 2006: Trajectory shifts in the Arctic and subarctic freshwater cycle. *Science*, **313**, 1061–1066, doi:[10.1126/science.1122593](https://doi.org/10.1126/science.1122593).
- Qian, Y., and Coauthors, 2015: Parametric sensitivity analysis of precipitation at global and local scales in the Community Atmosphere Model CAM5. *J. Adv. Model. Earth Syst.*, **7**, 382–411, doi:[10.1002/2014MS000354](https://doi.org/10.1002/2014MS000354).
- Screen, J., and I. Simmonds, 2010: The central role of diminishing sea ice in recent Arctic temperature amplification. *Nature*, **464**, 1334–1337, doi:[10.1038/nature09051](https://doi.org/10.1038/nature09051).
- Serreze, M., and R. Barry, 2011: Processes and impacts of Arctic amplification: A research synthesis. *Global Planet. Change*, **77**, 85–96, doi:[10.1016/j.gloplacha.2011.03.004](https://doi.org/10.1016/j.gloplacha.2011.03.004).
- Shepherd, A., D. Wingham, and E. Rignot, 2004: Warm ocean is eroding West Antarctic Ice Sheet. *Geophys. Res. Lett.*, **31**, L23402, doi:[10.1029/2004GL021106](https://doi.org/10.1029/2004GL021106).
- Singh, H., C. Bitz, A. Donohoe, J. Nusbaumer, and D. Noone, 2016a: A mathematical framework for analysis of water tracers. Part II: Understanding large-scale perturbations in the hydrological cycle due to CO₂ doubling. *J. Climate*, **29**, 6765–6782, doi:[10.1175/JCLI-D-16-0293.1](https://doi.org/10.1175/JCLI-D-16-0293.1).
- , —, J. Nusbaumer, and D. Noone, 2016b: A mathematical framework for analysis of water tracers. Part 1: Development of theory and application to the preindustrial mean state. *J. Adv. Model. Earth Syst.*, **8**, 991–1013, doi:[10.1002/2016MS000649](https://doi.org/10.1002/2016MS000649).
- Skific, N., J. Francis, and J. Cassano, 2009: Attribution of projected changes in atmospheric moisture transport in the Arctic: A self-organizing map perspective. *J. Climate*, **22**, 4135–4153, doi:[10.1175/2009JCLI2645.1](https://doi.org/10.1175/2009JCLI2645.1).
- Slonaker, R., and M. V. Woert, 1999: Atmospheric moisture transport across the Southern Ocean via satellite observations. *J. Geophys. Res.*, **104**, 9229–9249, doi:[10.1029/1999JD900045](https://doi.org/10.1029/1999JD900045).
- Sodemann, H., and A. Stohl, 2009: Asymmetries in the moisture origin of Antarctic precipitation. *Geophys. Res. Lett.*, **36**, L22803, doi:[10.1029/2009GL040242](https://doi.org/10.1029/2009GL040242).
- Sorteberg, A., and J. Walsh, 2008: Seasonal cyclone variability at 70°N and its impact on moisture transport into the Arctic. *Tellus*, **60A**, 570–586, doi:[10.1111/j.1600-0870.2007.00314.x](https://doi.org/10.1111/j.1600-0870.2007.00314.x).
- Turner, J., J. Overland, and J. Walsh, 2007: An Arctic and Antarctic perspective on recent climate change. *Int. J. Climatol.*, **27**, 277–293, doi:[10.1002/joc.1406](https://doi.org/10.1002/joc.1406).
- Vázquez, M., R. Nieto, A. Drumond, and L. Gimeno, 2016: Moisture transport into the Arctic: Source-receptor relationships and the roles of atmospheric circulation and evaporation. *J. Geophys. Res. Atmos.*, **121**, 13 493–13 509, doi:[10.1002/2016JD025400](https://doi.org/10.1002/2016JD025400).
- Wehner, M., and Coauthors, 2014: The effect of horizontal resolution on simulation quality in the Community Atmospheric Model, CAM5.1. *J. Adv. Model. Earth Syst.*, **6**, 980–997, doi:[10.1002/2013MS000276](https://doi.org/10.1002/2013MS000276).
- Werner, M., M. Heimann, and G. Hoffmann, 2001: Isotopic composition and origin of polar precipitation in present and glacial climate simulations. *Tellus*, **53B**, 53–71, doi:[10.3402/tellusb.v53i1.16539](https://doi.org/10.3402/tellusb.v53i1.16539).
- Winschall, A., S. Pfahl, H. Sodemann, and H. Wernli, 2014: Comparison of Eulerian and Lagrangian moisture source diagnostics—The flood event in eastern Europe in May 2010. *Atmos. Chem. Phys.*, **14**, 6605–6619, doi:[10.5194/acp-14-6605-2014](https://doi.org/10.5194/acp-14-6605-2014).
- Woods, C., R. Caballero, and G. Svensson, 2013: Large-scale circulation associated with moisture intrusions into the Arctic during winter. *Geophys. Res. Lett.*, **40**, 4717–4721, doi:[10.1002/grl.50912](https://doi.org/10.1002/grl.50912).
- Yang, B., and Coauthors, 2013: Uncertainty quantification and parameter tuning in the CAM5 Zhang–McFarlane convection scheme and impact of improved convection on the global circulation and climate. *J. Geophys. Res. Atmos.*, **118**, 395–415, doi:[10.1029/2012JD018213](https://doi.org/10.1029/2012JD018213).
- Yu, L., and R. Weller, 2007: Objectively analyzed air-sea heat fluxes for the global ice-free oceans (1981–2005). *Bull. Amer. Meteor. Soc.*, **88**, 527–539, doi:[10.1175/BAMS-88-4-527](https://doi.org/10.1175/BAMS-88-4-527).
- Zhang, X., J. He, J. Zhang, I. Polyakov, R. Gerdes, J. Inoue, and P. Wu, 2013: Enhanced poleward moisture transport and amplified northern high-latitude wetting trend. *Nat. Climate Change*, **3**, 47–51, doi:[10.1038/nclimate1631](https://doi.org/10.1038/nclimate1631).